

Static and fluctuating zigzag order, and possible signatures of Kitaev physics, in torque measurements of α -RuCl₃

S. Froude-Powers, Subin Kim, Jacob Gordon, Hae-Young Kee, Young-June Kim, and S.R. Julian*

Department of Physics, University of Toronto, Toronto, Ontario, M5S 1A7 Canada

(Dated: December 23, 2023)

We have measured magnetic torque on a $T_N = 7$ K single crystal of α -RuCl₃, as a function of the field angle in the ab -plane, focusing on temperatures between 2 and 20 K and fields from 0 to 9 T. We find a number of features, many of which can be classified by their angular periodicity. The sample shows an oscillation with a period of 180° (i.e. two-fold periodicity) and within the magnetically ordered zigzag phase there is a 60° period (i.e. six-fold) sawtooth pattern, which can be explained by reorientation of the zigzag domains as the crystal rotates in the applied field. We argue that the six-fold sawtooth and the two-fold sinusoidal signals arise from distinct regions of the crystal. Suppressing the zigzag order with an applied field above ~ 8 T at low temperature, a six-fold *sinusoidal* signal remains, suggesting that there is fluctuating zigzag order in the putative field-induced quantum spin liquid state. Finally, in testing theoretical results which predict a torque response with divergent slope across C_2 -preserving b -axes (B1-axis), we find no features like that predicted for Ising topological order. Instead we find features at low temperatures and fields just above the zigzag phase across the non- C_2 -preserving b -axes (B2-axes). Interpretation of this feature is complicated by the development of other similar signatures nearby at slightly lower fields, and by clear enhancement with thermal cycling. Additionally, we contrast the torque response of $T_N \sim 7$ K and 14 K samples.

I. INTRODUCTION

Quantum spin liquids have generated interest both as a new phase of condensed matter and for their potential applications in the fields of quantum computing and spintronics, where they offer a paradigm-shifting alternative to traditional electronics. The recent incorporation of spin-orbit coupling has played a key role [1–4], by making *topological* quantum spin liquids theoretically possible. The analytically solvable Kitaev model, with bond-dependent Ising-type interactions of $J_{\text{eff}} = 1/2$ nearest-neighbours on a 2D honeycomb lattice, leads to frustrated spins and an emergent topological quantum spin liquid (QSL) [5]. With no applied magnetic field this QSL is found to host emergent excitations of gapless Majorana fermions and gapped Z_2 vortices - novel excitations should they be found in nature. The possibility of realizing the Kitaev model in real materials has aroused considerable interest (for reviews see [6–10]), and of the various candidate materials α -RuCl₃, which is the focus of this paper, has been the subject of several experimental and theoretical studies.

The Kitaev Spin Liquid ground state has limited stability in the presence of competing exchange interactions, and at zero field α -RuCl₃ displays zigzag antiferromagnetic order below $T_N \sim 7$ K (Fig. 1c). The current understanding is that a minimal description must include a ferromagnetic nearest-neighbour Kitaev interaction, Heisenberg interactions extending to at least the third neighbours, and an off-diagonal Γ term [11] that couples nearest-neighbour spins (see e.g. [12] for a dis-

cussion, and [13] for x-ray scattering results determining the interaction strengths).

Above a modest field of ~ 7.5 T applied in the ab -plane, neutron diffraction shows that zigzag order is suppressed [16], and intense interest has focused on the magnetic field range $7.5 \text{ T} \lesssim B \lesssim 11 \text{ T}$, which we refer to as the “intermediate field phase”. This interest is enhanced by measurements that are consistent with predictions that a Kitaev spin liquid in an applied field will be a chiral spin liquid, with a gap that closes for fields parallel to certain high symmetry directions [17–19]. In particular, thermal Hall measurements showed a half-integer quantized thermal Hall effect [20], which is an expected signature of this phase. Moreover, angle- and field-resolved specific heat measurements, in the intermediate field phase [19], were interpreted in terms of gapped quasiparticle excitations, with a gap that closes when the applied field is parallel to the Ru-Ru bonds, as predicted by theory [5]. (Fig. 1a shows a schematic of the bond directions.) Other evidence for Kitaev physics includes temperature dependence of specific heat measurements [16, 21–23] showing a predicted double-peak structure in $C(T)$, although only the upper peak, near 100 K, has the predicted release of $0.5 R \ln 2$ expected for Majorana fermions.

The quantized thermal Hall effect measurements have been difficult to reproduce outside a few labs [24, 25], and alternative explanations have been suggested for the origin of the result, including phonons [26] and topological magnons [27]. Thus there is a clear need for other measurements that could show signatures of a field-induced topological spin liquid.

Our particular motivation for measuring the torque was a prediction by some of us [17], summarized in §IV:E, that the angle-resolved torque response of a state with

* stephen.julian@utoronto.ca

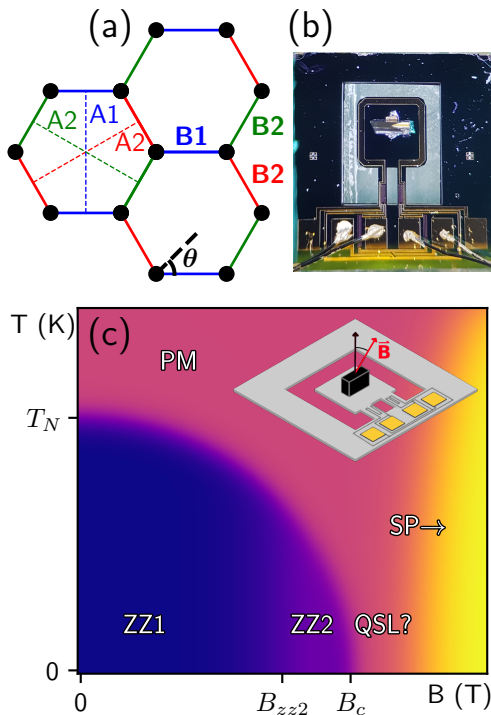


FIG. 1: (a) The three X,Y,Z Ru-Ru bond directions of α -RuCl₃: the *b*-axes are B1 (the C_2 axis for a crystal with monoclinic symmetry), and two equivalent B2 axes. For $R\bar{3}$ symmetry, B1 and B2 are equivalent. The complementary *a*-axes, A1 and A2, are shown as dashed lines. The nomenclature is borrowed from Lampen-Kelley et al. [14]. (b) Top view of our large $T_N \sim 7$ K sample (sample L7K) mounted on the Quantum Design torque chip P109A. (c) Cartoon phase diagram of α -RuCl₃. Above the zigzag ordering temperature $T_N \simeq 7$ K, α -RuCl₃ is in the paramagnetic (PM) phase. At zero field, below T_N α -RuCl₃ has zigzag antiferromagnetic order (ZZ1). Increasing the field beyond a threshold B_{zz2} induces a new zigzag ordering (ZZ2) [15]. Zigzag order is suppressed for fields beyond $B_c \sim 7.5$ T, at high field reaching a field-induced spin-polarized (SP) state. Inset: Cartoon depicting the angle-resolved torque magnetometry setup. The arrows represent the field direction, and the vector for the magnetic moment of α -RuCl₃.

Kitaev Ising topological order, of the kind consistent with the fractional thermal Hall measurements, should have a negative slope at any in-plane C_2 -symmetry-preserving axis, e.g. the B1-axis for a crystal with C_2/m -symmetry (defined in Fig. 1a), with the slope becoming more negative as $T \rightarrow 0$ K. This prediction is made for a generic spin model [11].

In this study we report on the magnetization of α -RuCl₃ through measurements of the angle-resolved torque, τ , in applied in-plane fields of up to 9 T in the temperature range of 2 - 20 K. We have measured several single crystals and find that the torque behaviour is

sample dependent.

There have been several recent investigations into the low-temperature structure of α -RuCl₃ which have clarified the different T_N reported in the literature (from 6.5 K to 14 K) [28–30]. Samples with $T_N \sim 7.5$ K have been shown to represent the highest quality samples with $R\bar{3}$ symmetry at low temperature, minimal stacking faults and very low levels of C_2 contamination, while samples with $T_N < 7$ K have a mixture of $R\bar{3}$ and C_2 regions and a high density of stacking faults, while $T_N > 10$ K samples have ABAB stacking, as opposed to the ABCABC stacking of $T_N \sim 7$ K samples [22, 31].

In this paper we present results for a large, $T_N = 7$ K crystal. Below, and in the Appendices, we justify this choice, presenting results on the sample dependence of the torque, and the effects of thermal cycling.

Our study complements previous torque studies of α -RuCl₃, some of which focused on the torque or the related magnetotropic coefficient for out-of-plane applied fields ([32–34]), while the only previous torque study for in-plane fields that we are aware of seems, in light of our results, to have been affected by strong residual C_2 strains or disorder [35].

Our results are more complex than predicted for a pure Kitaev interaction: just outside the boundary of the zigzag phase we see a sinusoidal six-fold-symmetric signal, but rather than reflecting a closed gap along the Ru-Ru bond direction, it may be indicative of short-range fluctuating zigzag order. At low temperature, however, a sharp signature with negative slope is observed at the B2-axes (defined in Fig. 1a) as soon as the intermediate phase is entered from the zigzag phase. This signature’s similarity to the theoretical results [17] may be misleading, however, given its location along the non- C_2 -preserving B2-axes, as well as being enhanced with thermal cycling, implying extrinsic origins.

We also report, within the zigzag phase, the existence of strong sawtooth steps with six-fold symmetry and, at all fields at all temperatures, a two-fold torque signal that is sample and also sample-history dependent, which leads us to conclude that the two-fold signal is probably not intrinsic.

II. EXPERIMENT

We measured single crystals of α -RuCl₃ that were grown using chemical vapor transport as described in previous work [26]. Two grams of α -RuCl₃ powder (Sigma-Aldrich, Ru 45-55%) were sealed in a quartz tube under vacuum. The quartz tube was heated in a two zone furnace where the temperature gradient was kept at 70 °C. The powder was initially heated at 850 °C for two days, followed by cooling at 4 °C/h down to 600 °C.

In all we checked the torque response of 14 single crystals, thirteen of which were “small”, measuring $\sim 100 \times 50 \times 50 \mu\text{m}^3$, suitable for measurement with miniature piezoresistive cantilevers (Seiko Instruments PRC120).

The most extensive set of measurements was done on a “large” single crystal, measuring $\sim 1 \times 0.6 \times 0.3 \text{ mm}^3$, with a 7 K transition (sample L7K), placed on a Quantum Design Torque Chip P109A (Fig. 1b). For reasons presented below, and in the Appendices, we believe this to be the highest quality sample, and it is thus the focus of this paper. The crystal was held in position on the PPMS chip by an L-bracket of copper sheet and a light layer of vacuum grease (as shown in Fig. 1b), with the c^* -axis aligned within 2° of the axis of rotation, which was perpendicular to the magnetic field. This sample (L7K) has additionally been characterized with x-ray diffraction to confirm its orientation.

All measurements were done using a Quantum Design PPMS, using the Horizontal Rotator option, at temperatures between 2 and 20 K, and fields from 0 to 9 T. In the majority of our measurements the crystal was rotated such that the applied field swept through 180° or 360° in the ab -plane, while the temperature and the magnitude of the field were held constant. These angular sweeps were done in the same direction in all measurements presented here. In all of the 360° studies the torque consisted very precisely of two repeated 180° patterns, as expected. In most cases we also swept temperature at fixed angle, to check T_N (see Appendix §D). We checked for hysteresis by reversing the direction of rotation and found none within our measurement resolution.

In all of our plots, angles have been translated so that 0° and -180° are at the B1 axis. Moreover, torque is given in volts (or volts per tesla) which was the signal from a Wheatstone bridge that measured the twisting of the sample platform. A calibration measurement, outlined in the Appendix (§C), provides a conversion factor of $(17 \pm 4) \times 10^9 \text{ Nm}^{-2}/\text{V}$ between these voltages and the torque density in Nm^{-2} .

The absence of hysteresis, and calculations outlined in Appendix C, demonstrate that the features that we observe in the torque arise in the magnetic moments of our sample, with minimal contamination of the signal by non-linear “torque interaction” [36] effects.

III. RESULTS

Our torque signals can be decomposed into oscillations with distinct periods as a function of angle, and in this section we discuss them in sequence starting with two-fold (180° period) signals, before turning to six-fold signals which are a focus of later discussion. We finally discuss sharp features of the ordered, and then intermediate field, phases. A special focus is put on features near high-symmetry field angles, such as the B2 axis where at low temperatures in the intermediate field phase we see large step-like features develop.

180° Periodic Signal: A clear 180° periodic signal appears in all of our torque vs. angle measurements. Fig. 2 shows a baseline series of measurements at 20 K at fields between 4 and 9 T on sample L7K, in which a 180° signal,

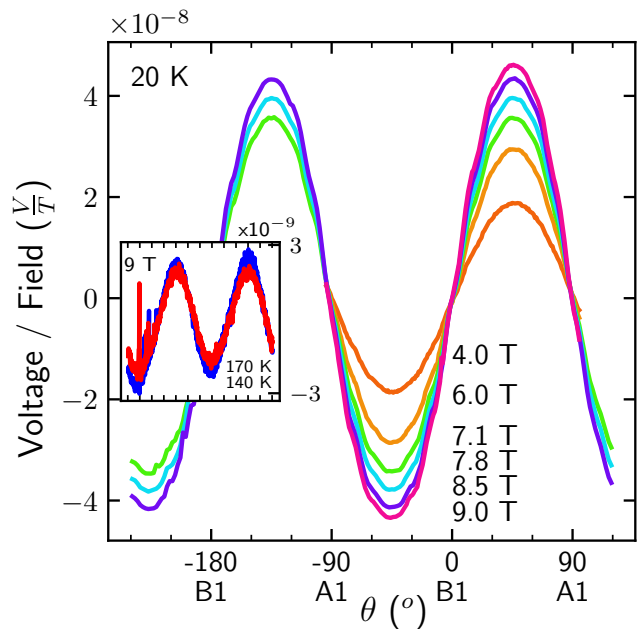


FIG. 2: At 20 K the torque is dominated by a clear 180° (i.e. two-fold) signal that grows strongly with field. At all fields this acts as a significant background to the more interesting higher-frequency signals. Inset: 9 T measurements at 140 K and 170 K, showing that the two-fold signal persists up to the structural transition. For sample L7K the conversion from voltage to torque in all plots is $2.77 \pm 0.09 \text{ Nm}/\text{V}$, while the magnitude of the static moment perpendicular to the applied field can be obtained from $1.0 \times 10^{-7} \text{ V}/\text{T} \leftrightarrow (0.019 \pm 0.001) \mu_B$ per formula unit (see Appendix §C for details).

that scales with field as B^2 , dominates the torque. This 180° background signal reveals the presence of regions of our crystal with C_2 symmetry. (In the Discussion we argue that these regions coexist with $R\bar{3}$ regions.) The angle-resolved torque vanishes at both the B1 and A1 axes. In all of our plots we have shifted the origin of the horizontal axis so that B1 is at 0° and -180° , while A1 is at $\pm 90^\circ$. As shown in the inset of Fig. 2, the 180° periodic contribution persists up to at least $\sim 140 - 160$ K [37].

The 180° periodic signal is moderately enhanced as $T \rightarrow 0$ K. This can be seen in Fig. 3a, which shows the angle-dependent torque at 4 T at various temperatures. Additionally, with decreasing temperature a pronounced six-fold (60°) contribution appears. Fig. 3b shows the temperature dependence of the Fourier amplitudes corresponding to the 180° and 60° components. It is evident that these components are independent. From this we justify the choice to individually fit and subtract off the temperature and field dependent 180° sinusoidal component for each dataset in our future analyses and plots.

60° Periodic Signal: We turn now to the 60° periodic signals. These signals are very prominent in our sample

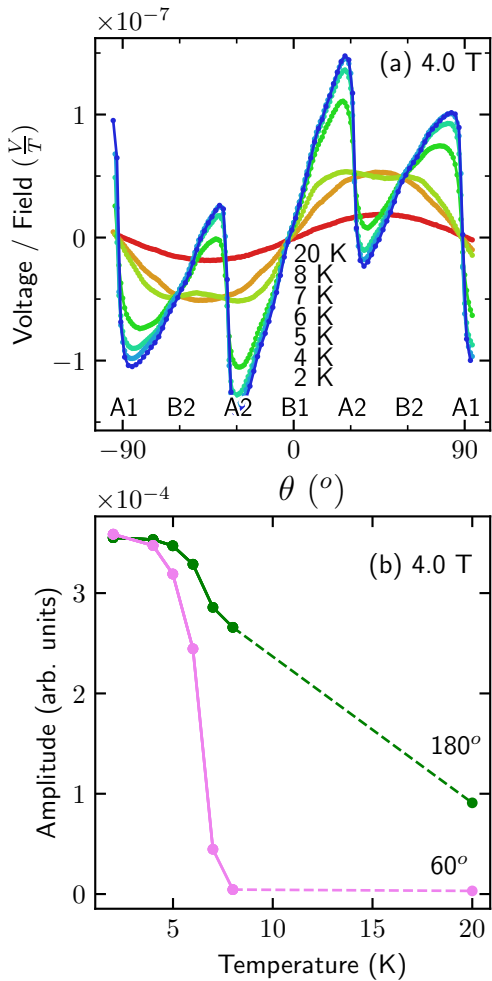


FIG. 3: (a) Angle-resolved torque measurements at 4 T for $2 \text{ K} < T < 20 \text{ K}$. A nearly pure 180° periodic signal for $T \gg T_N$ is distorted starting at $\sim T_N$, gaining a 60° periodic signal which quickly transforms into a sawtooth pattern. (b) Fourier amplitudes of the 180° (green) and 60° (pink) periodic contributions to the signal in (a), plotted against temperature. The 60° periodic contribution activates abruptly at $T \sim T_N$.

within the zigzag ordered phase, but only for sufficiently strong fields. For example, as seen in Fig. 4, at 2 K (i.e. deep within the zigzag ordered phase) the torque at 0.5 T, after a subtraction of the two-fold contribution, is nearly constant with no notable features, while a field of 1.2 T induces a weak 90° periodic contribution whose origin is unclear. At 4 T, however, the six-fold sawtooth pattern emerges very clearly. In Fig. 3b it can be seen that the Fourier amplitude of the 60° periodic component is negligible for $T > T_N$, but grows rapidly upon entering the zigzag phase. Fig. 4 shows that increasing the strength of the applied field beyond $\sim 6 \text{ T}$ within the zigzag phase distorts the signal from a clean sawtooth, with the step-like features increasing in amplitude across the A1-axis, while decreasing across the A2-axes. We dis-

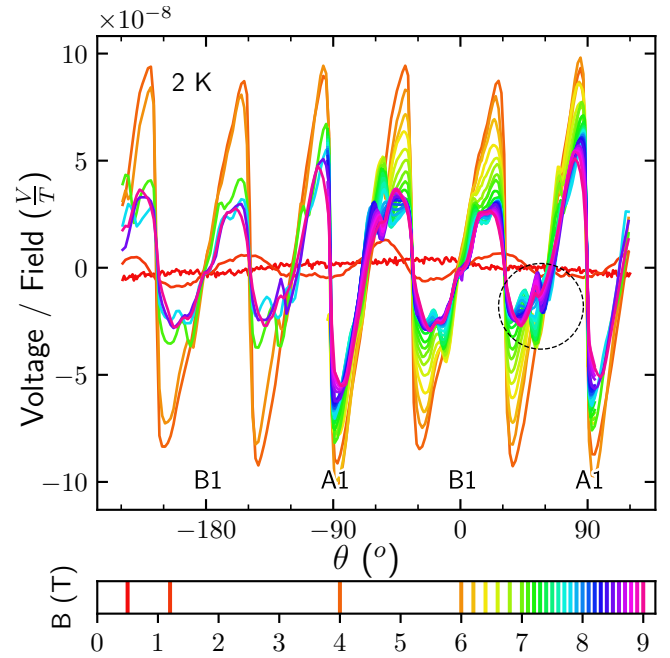


FIG. 4: Angle-resolved torque of L7K at 2 K. A temperature-dependent 180° periodic sine wave contribution has been subtracted. At low field the torque response is constant, as expected. A 90° periodic contribution is present at 1.2 T, and the signal further develops into a 60° periodic sawtooth signal by 4 T. The sawtooth discontinuities are present at each equivalent a -axis (ie. $\pm 30^\circ$, $\pm 90^\circ$, ...). The sawtooth signal distorts as field strength is increased, with intermediate features developing between each discontinuity, and with the overall signal amplitude decreasing. Inflection points form along the b -axes (ie. 0° , $\pm 60^\circ$, ...) with increasing field, which invert across the B2-axes ($\pm 60^\circ$, $\pm 120^\circ$) upon exiting the zigzag phase. The circled region is discussed below as a possible signature of Kitaev physics (see §IV-D).

cuss the implication of this distortion with respect to a coupling of the 180° and 60° periodic contribution to the signal in §IV:C. The sawtooth signal is fully suppressed at $\sim 8 \text{ T}$, as the intermediate field phase is entered. This same trend can be seen at other temperatures $T < T_N$ in Fig. 5(a-d), where the signatures of a sawtooth signal can be seen up to 7.8 T at temperatures as high as 6 K.

We argue in §IV:A that this sawtooth signal arises from rotation of zigzag domains as the sample rotates in the applied field, and that it is thus an indicator of good sample quality. There we show that the steps of the sawtooth signal are expected to align with the a -axes (i.e. A1 and A2 of Fig. 1a). We note that the orientation determined this way is consistent with x-ray diffraction at room temperature. Locating the a -axes at the steps in the sawtooth, together with the alignment of the zero-crossings of the torque with the B1- and A1-axes at 20 K, determines the orientation of our crystal at low temperature.

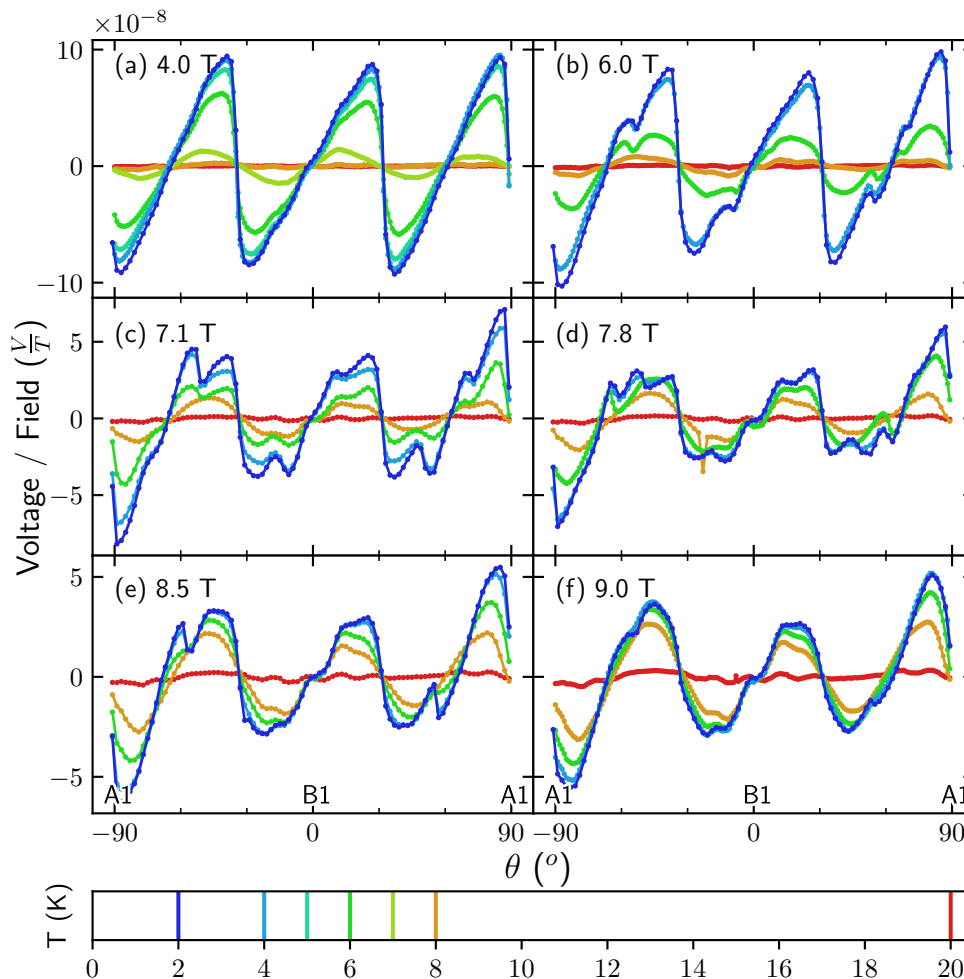


FIG. 5: Torque vs. angle in sample L7K at fixed fields, vs. temperature. A 180° sinusoidal contribution has been subtracted. (a) 4 T. At 8 K and above no features are present; 7 K shows a 60° sinusoidal contribution, without harmonic distortion. Below 7 K the sawtooth pattern grows rapidly. (b-d) 6, 7.1 and 7.8 T. The sawtooth steps weaken with increasing field, as a sinusoidal pattern emerges at higher temperatures. A complex pattern of intermediate local extrema appears. The sharp step at the A1-axes ($\pm 90^\circ$) may be due to harmonic distortion of the two-fold contribution. At the B1-axis (0°) a plateau appears and grows with increasing field. (e-f) The step at the A1-axes, and plateau at the B1 axis, persist. Several of the local extrema have decayed or disappeared, but a sharp peak, or step-like discontinuity, emerges near B2 ($\sim \pm 60^\circ$) at 8.5 T.

A novel finding of this study, presented in Fig. 5, is that a sinusoidal 60° torque signal persists outside of the zigzag phase, within the putative intermediate field Kitaev state. At 4 T a six-fold sinusoidal signal can be seen in a narrow temperature range below 7 K, within the zigzag phase, as in Fig. 5a. At higher fields, but still with $B < B_c$, the temperature range expands: the sinusoidal signal now appears at higher temperatures *outside* the zigzag phase, as well as at lower temperatures within the zigzag phase, before giving way to the sawtooth signal at still lower temperatures. Above B_c , again *outside* of the zigzag phase, the 60° sinusoidal signal persists down to the lowest temperatures measured.

Other features of the zigzag phase: The transition from zigzag order to the intermediate field phase is

complicated by an intervening zigzag phase, denoted as zigzag 2, as opposed to zigzag 1 at low field (see Fig. 1), with a critical field that varies strongly with field angle [38, 39]. In the region between about 6 and 7.7 T [38] where these transitions take place, we see in Fig. 5b-d sharp peaks whose position is field dependent. Plotting these features vs. field and angle, however, reveals a pattern with little similarity to the accepted phase boundaries [38] (see Fig. 15 in Appendix §E). If the origin of these peaks is in the complex zigzag phase boundaries shifting with changing in-plane field angle, it is notable that both the large and small $T_N = 7$ K sample host these complex features, though the domain rotation is seen only in sample L7K (see Fig. 13 in Appendix §B). The placement of these peaks, between high-symmetry

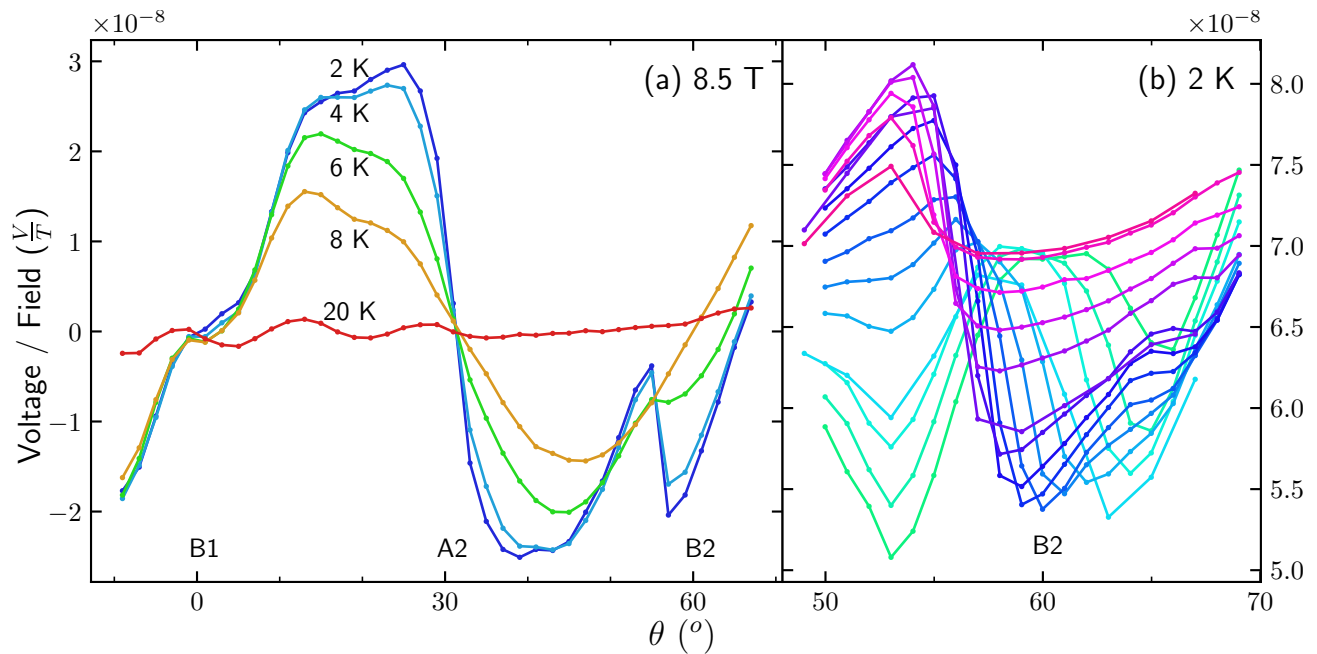


FIG. 6: (a) Zoomed-in window capturing the B1, A2, and B2 axes of sample L7K at 8.5 T. A 180° periodic sine wave has been subtracted. A plateau is seen across the B1-axis, and is only weakly temperature dependent. A steep slope develops across the A2-axis (just as across the A1-axis) with decreasing temperature. Near B2, below a threshold temperature ~ 4 K, a sharp feature with negative slope develops. (b) The raw (no background subtraction) data of the angle-resolved torque near the B2-axis at 2 K, for magnetic fields from 7.5 T (green) to 9.0 T (purple) at evenly spaced intervals of 100 mT. The steep sloped feature develops quite suddenly upon entry into the intermediate field phase, and is seen to move as the field changes.

axes instead of along them, as well as their complex dependence on field strength and direction make it difficult to assess them further with only the measurements conducted. However, in §IV:B we present the possibility that they arise from zigzag domain switching in C2 regions, in contrast to the periodic six-fold sawtooth pattern that, we will argue, arises in $R\bar{3}$ regions of our sample. In the remainder of this section we focus on the peaks near high-symmetry field-angles in the intermediate field phase.

Features of the Intermediate Field Phase: In Fig. 5d, e and f we see features in the immediate neighbourhood of the A1, B1, and especially, the B2 axes. At A1 there appears to still be a downward step, but we argue below that this is due to a combination of non-linear distortion of the magnetization and torque, and subtraction of a pure 180° sinusoidal contribution (see Fig. 10). In Fig. 6a we focus on the temperature evolution of B1 and B2 features at 8.5 T. At the zero-crossing marking the B1-axis (0°) the signal shows a plateau for temperatures below 8 K. Figures 7a,b show the signal at B1 with both a 180° and a 60° periodic sine wave subtracted, showing that a negative slope in the residual signal across the B1-axis is enhanced with decreasing temperature (Fig. 7a), but that it is not field dependent for $B > 7.5$ T (Fig. 7b), so we conclude that it is not a particular feature of the intermediate field phase.

In contrast, across the B2-axes a steep negative slope

forms in the torque response that is only seen in the intermediate field phase at the lowest temperatures. At the B2 axes at 8.5 T, for example, there is an asymmetric, downward peak at $\sim 60^\circ$ whose left-hand side appears to be a discontinuous step, but that shows up only at 4 and 2 K (Figs. 5e, 6a), while Figs. 6b and 5c-e show that, at 2 K, the feature grows rapidly as the field is increased beyond 7.5 T. This signal near the B2 axis is enhanced and shifted slightly after thermally cycling the sample, as seen in Appendix §A. A comparison of this feature to the theory for a Kitaev spin liquid at high field is made in §IV:D.

Finally, clear oscillations, with weak temperature and field dependence, appear within $\pm 60^\circ$ of B1 and A1 (see e.g. Fig. 5c-f, or the 20 K line in Fig. 6a). These oscillations are small compared to the 180° and, at low temperature, the 60° periodic components. They are also weak compared to the features that develop between axes in the zigzag phase, and also the sharp feature which develops across the B2 axis in the intermediate field phase. These small features are distinct from the temperature dependent, though field independent, feature that is seen (after successive 180° and 60° periodic subtractions) across the B1 axis. Although we do not understand these weak oscillatory features, we do not discuss them further, as they are evidently inherent to neither the ordered phase nor the intermediate field phase.

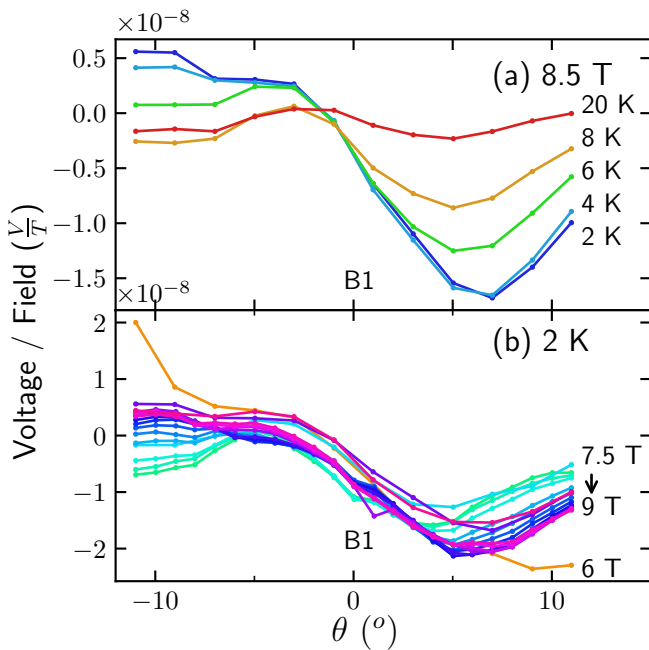


FIG. 7: (a) Angle-resolved torque about the B1 axis at 8.5 T and temperatures from 20 K (red) to 2 K (blue), (b) Angle-resolved torque about the B1 axis at 2 K and fields at 6 T (orange), and from 7.5 T (teal) to 9 T (purple). In addition to a 180° sine wave subtraction, a further 60° periodic sine wave has been subtracted.

IV. DISCUSSION

First we discuss the origin of the sawtooth pattern seen within the zigzag-ordered phase because this allows us to unambiguously determine the orientation of the crystal, and the sign of the torque. We follow this with a brief discussion of the origin of the 180° periodic signal, concluding that the sawtooth and two-fold signals arise in physically separate parts of the sample. We then discuss the non-sawtooth 60° periodic sinusoidal signal which develops in proximity to the antiferromagnetic region and persists into the intermediate field phase. Finally, the fine structure seen at the lowest temperatures with increasing field are discussed, focusing on the features that develop near the B1 and, especially, the B2 axes, and their possible connection to theoretical predictions for a Kitaev spin liquid.

A. Interpretation of the saw-tooth pattern

Crystal L7K shows a strong, six-fold, saw-tooth pattern in the zigzag ordered phase (see for example the 2 K curve in Fig. 3).

If the cantilever used in a torque measurement is too soft, sawtooth steps can arise even when the underlying magnetization is sinusoidal, a non-linear experimental artifact known as “overcritical torque interaction” [36]. We establish in Appendix C that we are far from the overcritical regime, and thus that the sawtooth steps in the torque are indeed coming from the magnetization of the sample.

The basic physics of this pattern can be understood using a simplified free energy

$$\mathcal{F}_i = F_{zz,i} - \vec{M} \cdot \vec{B} \quad (1)$$

$$\text{where } F_{zz,i} = J_{zz}(\vec{M}_{A,i} \times \hat{b}_i) \cdot (\vec{M}_{B,i} \times \hat{b}_i)$$

$$\text{and } \vec{M} = (\vec{M}_{A,i} + \vec{M}_{B,i}).$$

The subscript $i = (1, 2, 3)$ labels three possible orientations of the zigzag domains (see Fig. 8(a)). The \hat{b}_i are unit vectors parallel to the three Ru-Ru bond-directions, and in each zigzag domain there are two sublattices, A and B, with magnetization per formula unit (f.u.) $\vec{M}_{A,i}$ and $\vec{M}_{B,i}$. The cross product with the unit vector \hat{b}_i thus gives the component of the sublattice magnetization that is perpendicular to the i^{th} Ru-Ru bond-direction, so the J_{zz} term in Eq. 1 stabilizes zigzag order with the moments perpendicular to \hat{b}_i .

For a given direction of \vec{B} within the plane, we minimize the three \mathcal{F}_i 's numerically, with respect to the directions of $\vec{M}_{A,i}$ and $\vec{M}_{B,i}$, assumed for simplicity to lie within the ab -plane. For this calculation we fixed the magnitude of M_A and M_B at $0.35\mu_B/\text{f.u.}$, which is representative of measured static in-plane moments in the zigzag phase [22, 40–43], while the zigzag exchange constant was set to $J_{zz} = 1.85k_B/(0.35\mu_B)^2$, which causes the zigzag order to collapse at around $B = 8$ T.

At zero field (Fig. 8a) the sublattice magnetizations are purely perpendicular to the bond, for each domain, and the free energies of the three domains are equal in the absence of C2 anisotropy. When a field is applied, however, the sublattice magnetizations acquire a component that is parallel to the field (upper row of Fig. 8b), giving rise to a non-zero net magnetization $\vec{M} = \vec{M}_A + \vec{M}_B$. The free energies of the three domains are then no longer equal, rather the free energy of each domain acquires a sinusoidal dependence on the angle between \vec{B} and \hat{b}_i , as can be seen in Fig. 8c.

The results are shown in Fig. 8c-e. As the field rotates, the minimum free energy switches from one domain to the next whenever the field passes through an a -axis. From the minimum $\mathcal{F}_i(\theta)$ at a given field angle θ we can calculate the magnetization \vec{M} and the torque, $\vec{M} \times \vec{B}$. The resulting magnetization amplitude and torque are shown in Fig. 8d and e for $B = 3$ T. This field was chosen so that we could compare our calculated magnetization amplitude with the measured magnetization in Fig. 3g of Balz et al. [38] (blue points in Fig. 8d).

In Fig. 8c the domain in which \hat{b}_i is most parallel to \vec{B} has the lowest free energy. This is because for this

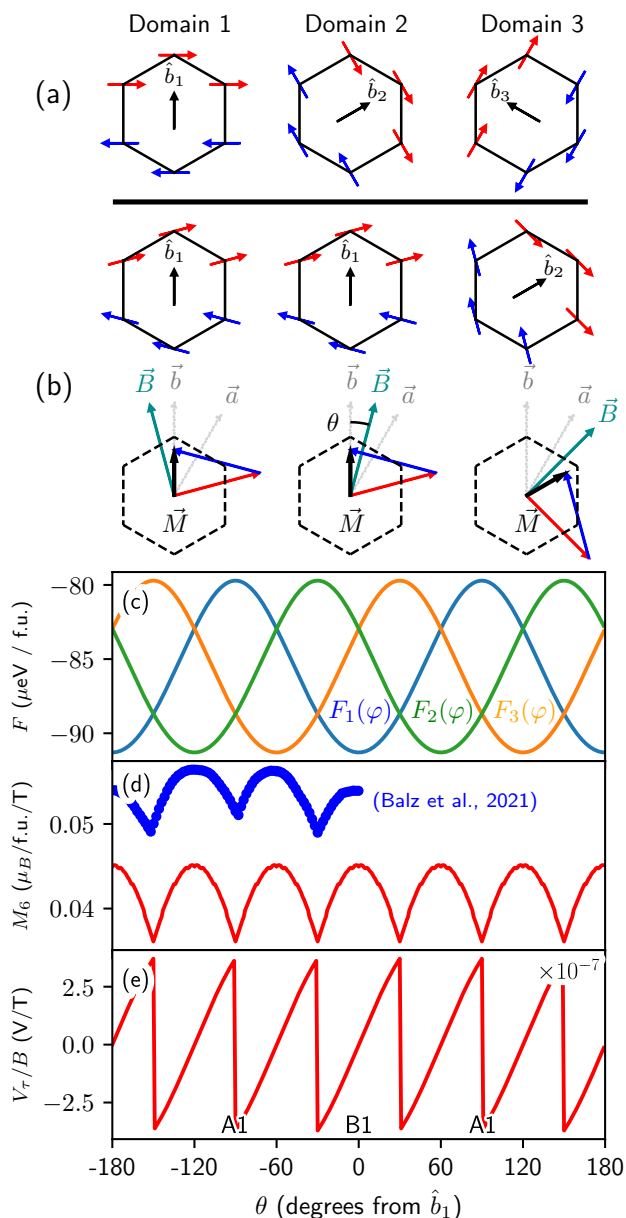


FIG. 8: (a) The three equivalent zigzag spin domains at zero field. The exchange energy in our simplified model depends only on the component of the magnetization that is perpendicular to a Ru-Ru bond (i.e. to a b -axis). (b) In the presence of an applied field, the system switches domains to keep $\vec{M}_{\perp,i}$ as perpendicular to the applied field as possible, minimizing the exchange-plus-Zeeman energy. The net magnetization, \vec{M} , is given by the sum of the two sublattice magnetizations. As \vec{B} passes through an a -axis the magnetization \vec{M} switches from one side of \vec{B} to the other, causing a step in the torque. (c) Free energy, (d) magnetization (M_6), and (e) torque, calculated using a toy model of zigzag order as described in the text (Eq. 1). The filled blue circles in (d) are the digitized magnetization of Baltz et al. [38]. For (d,e), M_6 and τ have been converted into the units used in Ref. [44], and this paper, respectively.

zigzag domain both \vec{M}_A and \vec{M}_B can have a component parallel to \vec{B} , lowering the Zeeman energy, while remaining as antiparallel to each other as possible, minimizing the zigzag exchange energy. When the minimum free energy switches between one domain and the next, the net magnetization jumps from one side of \vec{B} to the other (Fig. 8b, lower row, middle and right figures), producing a step in the torque (Fig. 8e) and a cusp in the magnetization (Fig. 8d). For comparison with measured data, we have converted the calculated torque into the units used in this paper – volts per tesla: quantitatively our result is about 3.5 times larger than the observed sawtooth torque. This result is remarkably close given the simplicity of our model, and the assumption that our entire sample is pure $R\bar{3}$ symmetry.

Meanwhile the magnetization is presented in units of $\mu_B/\text{f.u.}/\text{T}$, which are the units used in Ref. [44], for which we calculate the two-fold torque in Appendix F. The conversion between emu/T (used in Ref. [38]) and $\mu_B/\text{f.u.}/\text{T}$ is approximately 9.3×10^{-3} for α -RuCl₃. The similarity of our model curve and the measured magnetization (“ M_6 ”) shows that the cusp in the measured magnetization vs. angle is also explained by domain rotation.

We note finally that Eq 1 is meant only as an illustration of the effect of zigzag domain rotation on the torque and magnetization, and not as a realistic model for α -RuCl₃. Improved agreement with measurement can be obtained by adding Heisenberg and other terms, but for illustrative purposes we keep things as simple as possible.

Thus, the sawtooth pattern in the torque is a dramatic result of the switching of zigzag domains as the field rotates, but this is consistent with earlier magnetization measurements, which have themselves been explained by more sophisticated theoretical modeling (e.g. [12]). This differs, however, from a recent interpretation of magneto-optical spectroscopy which argued that for $B \parallel \vec{a}$ the zigzag order ultimately rotates such that the spins are perpendicular to that a -axis [45]. This would not produce steps in the torque.

A sample in which the domain walls were pinned and unable to move would not produce a six-fold signal in the zigzag phase even if all three domains were equally stable at zero field; nor would a six-fold signal appear in a sample with single-domain zigzag order due, for example, to strong residual C_2 strain, as discussed below.

B. Two-Fold Contribution

All of the samples we measured exhibit a strong two-fold (i.e. a 180° period) signal. The results for sample LK7 are shown in §III (see Fig. 2), while results for our small samples (which tend to display more pure C_2 symmetry in their results) are shown in Appendix B. Previous studies have assumed that 180° periodicity, reflecting C_2 symmetry of the crystal, involves a shortened Ru-Ru bond along a primary b -axis [40], which in our notation

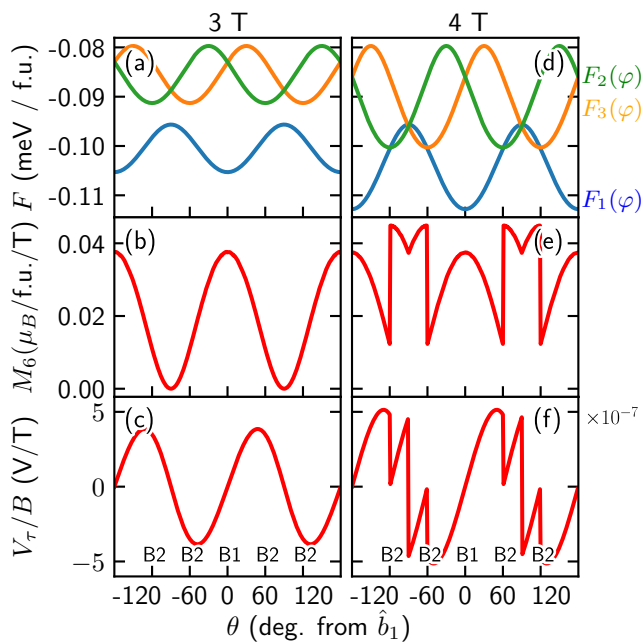


FIG. 9: The effect of breaking the degeneracy between the zigzag domain energies by making $J_{zz,1}$ 1.2 times larger than $J_{zz,2}$ and $J_{zz,3}$. The model is otherwise the same as in Fig. 8. (a), (b) and (c) show the free energy of the three domains, and the resultant magnetization and torque, at 3 T, while (d), (e) and (f) show the same quantities at 4 T. At 4 T the free energies now intersect at some angles, causing sawtooth steps and jumps in the magnetization.

would be the B1 bond. In the zigzag phase, only sample L7K shows the sawtooth torque, and a notable feature is that the sawtooth and two-fold signals seem to be simply additive.

We can add C_2 terms to Eq. 1 in two ways: 1) make J_{zz} larger along the B1 axis, or 2) add an explicit C_2 term such as $J_{C_2}[(\vec{M}_A \cdot \hat{b}_1)^2 + (\vec{M}_B \cdot \hat{b}_1)^2]$. The effect on the free energy is the same. Fig. 9a-c shows the free energy, magnetization and torque at 3 T when J_{zz} along \hat{b}_1 is increased by a factor of 1.2, while J_{zz} along the other axes is unchanged. As can be seen, the free energy of domain 1 is lowered, producing a sinusoidal two-fold torque. For this value of $J_{zz,1}$ the free energy of the most stable domain doesn't intersect that of the others, so there is no switching between domains, and the 6-fold sawtooth signal is gone. This would appear to be a possible model for the samples in which there is no sawtooth torque in the zigzag phase.

In Fig. 9d-f, we have increased the field to 4 T, which increases the amplitude of the sinusoidal variation in the free energy to the point where the free energies of domains 2 and 3 start to overlap with that of domain 1. This causes sawtooth steps in the torque, and dramatic jumps in the magnetization, but they do not have six-fold symmetry, the steps do not occur at the a -axes, and

clearly the two- and six-fold torque and magnetization are not simply additive. Figs. 9e and f look quite unlike magnetization measurements [44], but the steps in torque, not aligned with the A1 and A2 axes, offer a possible explanation of the steps that develop at intermediate angles, between 6 and 9 T (Fig. 5).

Non-linear interference between the two-fold and six-fold free energy terms, and notably moving the sawtooth steps away from the a -axes, is an unavoidable feature of any model where these contributions arise from the same set of magnetic moments, and so we reach the significant conclusion that the 6-fold sawtooth and the 2-fold signals in sample LK7 come from different regions of the sample: either completely phase separated, or perhaps as layered intergrowths that are intimately mixed. This is consistent with diffraction measurements [30] in α -RuCl₃ that see in some samples a mixture of $R\bar{3}$ and C_2/m regions.

In Appendix A it is shown that the 180° contribution is affected by thermally cycling the sample from low temperature to room temperature and back, while the sinusoidal 60° signals are not. This suggests to us that the 180° contribution is not intrinsic, but is instead a result of residual strain or accumulated impurity phases and stacking faults in the sample, perhaps either from cooling through the ~ 150 K structural transition too quickly, or from the way the crystals are mounted, with one end stuck to the cantilever with grease. Moreover, other measurements by some of us [29] support the notion that the intrinsic low-temperature structure is $R\bar{3}$ (see also [30]).

It seems that most studies on samples with predominantly $R\bar{3}$ symmetry still show varying degrees of residual C_2 symmetry at low temperature, and it may be that samples have to be cooled very slowly, in strain-free conditions, to show pure $R\bar{3}$ symmetry (e.g. [21, 38, 41]). As our measurements have already thermally cycled the sample, future study would be required to further explore this aspect of the low-T symmetry of high-quality α -RuCl₃.

C. Six-fold signal in the intermediate field phase

The sinusoidal 60° periodic signal appears to be a distinct but related phenomenon from the sawtooth signal seen in the zigzag phase. Both at the boundary to the zigzag phase at low fields, and at low-temperatures in the intermediate field phase, this sinusoidal signal persists where the sawtooth signal is absent. The presence of the sinusoidal six-fold signal at 4 T, just below the boundary to the zigzag phase, perhaps offers some insight to what the signal represents. We know that in this region static zigzag order has set in, and the existence of a six-fold signal tells us that the zigzag order has a preferred domain that depends on field direction, but the sinusoidal nature of the signal tells us that fluctuations are still large enough that all of the domains are partially populated, with populations that vary smoothly as

the direction of the field changes. Fig. 12f (in Appendix A) shows that, at 9 T, the six-fold sinusoidal signal in the intermediate field phase grows gradually below 20 K, before saturating below ~ 4 K. Given the same form of the signal just below T_N at 4 T, and at 9 T below 20 K, the most logical interpretation is that the six-fold signal outside the zigzag phase is due to fluctuating zigzag order.

A simplified model of the fluctuating order can be made using a Landau free energy with anisotropic six-fold susceptibility as well as C_2 symmetry breaking, of the following form:

$$\mathcal{F}(M, \theta, \phi) \simeq \frac{1}{2}(\chi_0 + \chi_2 \cos(2\phi) + \chi_6 \cos(6\phi))^{-1} M^2 - MB \cos(\theta - \phi), \quad (2)$$

where M is the net magnetization, θ is the angle of the applied field within the plane, ϕ is the angle that the net magnetization vector \vec{M} makes within the plane and the term in brackets multiplying M^2 is χ^{-1} . As usual, angles are measured from the B1 axis.

For a given field \vec{B} , \mathcal{F} is minimized with respect to M and ϕ , and the torque calculated from $\tau_z = M_x B_y - M_y B_x$.

In Fig. 10 we show sample results, where \mathcal{F} has been minimized numerically. An important point is that the anomalous behaviour at the A1 axis, which is apparent after a 180° background has been subtracted (see Fig. 10b) is explained by non-linear coupling between the χ_2 and the χ_6 terms, which produces harmonic distortion. If instead of Eq. 2 we use a linear prefactor for M^2 (i.e. of the form $(\chi_0^{-1} + \chi_2^{-1} \cos(2\phi) + \chi_6^{-1} \cos(6\phi))$), then this anomaly at A1 is not reproduced. While the non-linear coupling can have many sources, in this case it is probably just the non-linearity of M vs B as the magnetization approaches saturation. Thus, the enhanced peaks near the A1 axis, seen, for example in Fig. 5e and f, are not a special feature of the six-fold physics. This interpretation requires, incidentally, that the two-fold and at least some of the sinusoidal six-fold signals originate in the same regions of the crystal.

Short-range zigzag order outside of the zigzag phase is not surprising. After all, inelastic neutron scattering measurements see a strong six-fold anisotropy in the magnetic scattering well above T_N [46], while specific heat measurements (e.g. [23]) clearly show an upturn as T approaches T_N from above, which is a signature of fluctuating short-range order, while ESR measurements [47] also see six-fold variation in the ESR frequency at high field and low temperature. Nevertheless, we do not have an explanation for why such fluctuating order should be stronger at high field than at low field, that is, why we do not see a six-fold sinusoidal signal at 4 T for $T > T_N$, but we do see it at 6 T and above. Regarding the intermediate field phase in the limit as $T \rightarrow 0$ K, in the Introduction we mentioned specific heat measurements [19] that found an apparent gap-closing six-fold anisotropy with

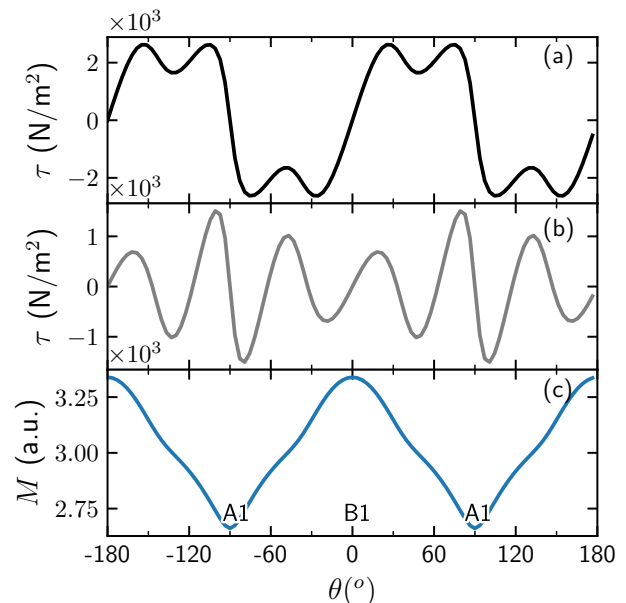


FIG. 10: (a) Torque density vs. angle for the free energy of Eq. 2. (b) After subtracting the two-fold contribution there is a downward step-like feature at $\pm 90^\circ$, as observed in the data at low temperature and high field (see Fig. 5e and f, and 13b). (c) Magnetization corresponding to (a).

an excitation gap that closes for $\vec{B} \parallel \vec{b}$. This was interpreted in terms of field-induced Kitaev Ising topological order, but our results suggest that fluctuating zigzag order should also be taken into consideration. A possible interpretation is that, because zigzag order is suppressed at 7.2 T for $\vec{B} \parallel \vec{a}$, as opposed to 7.7 T for $\vec{B} \parallel \vec{b}$ [38], then at 8 T, where specific heat measurements [19] see the strongest six-fold anisotropy, fluctuating zigzag order is largest along the b -axis simply because we are closer to the quantum critical point for suppression of zigzag order.

D. Comparison of torque signals in the intermediate phase with the theory for Kitaev Ising topological order

Theoretical Predictions: Kitaev [5] finds that, in an applied magnetic field, the itinerant Majorana fermions (MF's) of the Kitaev spin liquid become gapped, and they acquire a nontrivial Chern number. The resulting phase has Ising topological order (ITO).

The ITO is prohibited when the external field is parallel to a C_2 symmetry axis since the pseudo-mirror symmetry is unbroken. As the field sweeps across such a C_2 axis the Chern number switches from +1 to -1, and at the axis itself the gap must close. Gordon and Kee [17] noted that this topological transition leads to a sharp cusp singularity in the magnetotropic coefficient, which is independent of the details of microscopic spin interac-

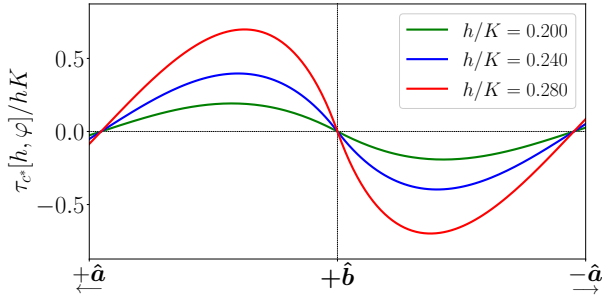


FIG. 11: Torque vs. angle calculated by Gordon and Kee [17].

tions, as this special C_2 symmetry is a property of the generic spin model. Writing the energy of the MF's as $\varepsilon_{\pm} = \pm\sqrt{(vq)^2 + m(\varphi)^2}$, where $m(\varphi)$ is the mass and v is the velocity of the MF's, the free energy at $T = 0$ is given by the integral over q of the lower branch:

$$\begin{aligned} \mathcal{F} &\simeq \frac{1}{2} \frac{A}{(2\pi)^2} \int_{vq < \Lambda} d\vec{q} \varepsilon_{-}(\vec{q}) \\ &= \frac{A}{12\pi v^2} \left[|m|^3 - (\Lambda^2 + m^2)^{3/2} \right], \end{aligned} \quad (3)$$

where $\Lambda \gg m$ is an ultraviolet cutoff and A is the area of the honeycomb unit cell. Gordon and Kee [17] focus on the singular $|m|^3$ part of \mathcal{F} , which yields a cusp in the magnetotropic coefficient, $\partial\tau/\partial\varphi$. This singular part may, however, be only weakly observable in the torque τ , which we obtain from:

$$\begin{aligned} \tau &= \frac{\partial\mathcal{F}}{\partial\varphi} = \frac{A}{2\pi v^2} \left[3m^2 - \frac{3}{2}(\Lambda^2 + m^2)^{1/2}m \right] \frac{\partial m}{\partial\varphi} \\ &\simeq -\frac{3A}{4\pi v^2} \Lambda m \frac{\partial m}{\partial\varphi}. \end{aligned} \quad (4)$$

The mass (i.e. the gap) is proportional to the angle between the applied field, φ , and the C_2 axis, φ_* : $m \propto \delta\varphi = \varphi - \varphi_*$. Thus, according to this calculation the torque at the C_2 axis passes through zero (as required by symmetry) but with a *negative* slope. The physics is relatively simple: the energy is lowered if the sample rotates the C_2 axis away from the field, because this increases the gap $m(\varphi)$, lowering the entire MF spectrum $\varepsilon_{-}(\vec{q})$. This expected behaviour is shown in Fig. 11.

Tanaka et al. [19] present strong evidence from specific heat for the closing of a gap at all of the b -axes in α -RuCl₃, which would be consistent with Ising topological order for $R\bar{3}$ symmetry. The closing of the gap is visible below about 5 to 10 K, but becomes increasingly clear as $T \rightarrow 0$ K. Thus, if Ising topological order is the relevant physics as opposed to, say, proximity to the zigzag quantum critical point, then in regions of our sample with $R\bar{3}$ symmetry we should expect that the torque acquires an increasingly negative slope at all three b -axes as the temperature is decreased below 10 K. On the other hand, in regions of our sample with C_2 symmetry then the increasingly negative slope would occur only at the B1 axis.

Both $R\bar{3}$ and C_2 regions of the crystal should contribute to a negative slope at our B1 axis, that appears in the intermediate field phase and grows with decreasing temperature.

Experimental Results: Within the zigzag-ordered phase we know that the slope of the torque is positive at the b -axes: from our model, the magnetization rotates *toward* the applied field in the zigzag phase. On the other hand, with the nearly pure 180° signal seen at 20 K (Fig. 2), the slope is positive at the B1 axis but weakly negative at B2.

To look for a negative slope in the intermediate field region at the B1 axis, we first subtracted the strong 180° signal, giving the results shown in Figs. 5 and 6. Even after this subtraction, however, we are left with the residual sinusoidal 60° signal discussed above, which has a positive slope at the B1 and B2 axes. In light of this we have also subtracted the six-fold sinusoidal signal in Fig. 7. After this subtraction the plateaus of Fig. 6 indeed yield a negative slope at the B1 axis, but the temperature dependence saturates below 4 K, rather than becoming increasingly negative, and the field dependence is even weaker: the residual negative slope persists deep into the zigzag phase (Fig. 7b), so the B1 axis torque does not appear to conform to the prediction for Ising topological order.

The B2 axis is not trivial to locate. We expect it to be at $\pm 60^\circ$, but perhaps due to interaction with the C_2 magnetization the magnetic B2 axis may be shifted to slightly lower angles compared to the crystallographic B2 axis. The approximate location of the isosbestic points (see Fig. 6a and b) suggests that the magnetic B2 axis, in the intermediate field phase, is located between 56° and 58°.

At that angle, within the zigzag phase (i.e. below 7.5 T) the slope is positive, but it rapidly becomes large and negative as the field increases to 8.5 T, before becoming smaller up to 9 T. Fig. 6 shows that at 8.5 T this feature corresponds to a sharp downward step that produces what appears to be a discontinuity in the torque across the B2 axis. Although this step is not smooth like the predicted torque pictured in Fig. 11, this may be due to the limited angular resolution in our measurement. The step has the negative sign predicted in the theory and it increases rapidly in size with decreasing temperature (see Fig. 6a), also as predicted. Moreover, although this step may look similar to the many peaks and steps that we see in Fig. 5 between 6 and 7.8 K, it is different in that: all of these other features fade upon entry into the intermediate field range, while this one is strongest in the intermediate field phase, just above the zigzag phase boundary. In this behaviour it is also different from the negative slope of the (background-subtracted) signal at the B1 axis. Thus this downward step has many of the theoretically predicted features for Ising topological order.

Fig. 9f, however, offers another explanation: this step may be due to domain switching in a C_2 region of the

crystal with a slightly higher critical field for suppression of zigzag order. This idea is reinforced by the fact that this feature grows upon thermal cycling of the sample to room temperature, as does the C2 signal (Appendix A). Thus, as the feature does not conform to the theoretical model, both by appearing along the ‘wrong’ axis (B2 instead of B1) and with the signal being enhanced after thermal cycling (see Appendix §A), it is likely not a signature of a field-induced Kitaev state. It would be worthwhile to explore it with other probes, especially direct measurements of the magnetotropic coefficient [32, 33] and the magnetization, but it may be sample dependent.

V. CONCLUSIONS

Comparing the torque vs. angle between three different samples, across a large region of the temperature-magnetic field phase space has led us to following conclusions.

1. Two-fold anisotropy of the magnetization is both sample dependent and sample-history dependent, and is probably not intrinsic to the true crystallographic ground state of α - RuCl_3 .
2. Within the zigzag ordered phase, high quality crystals show a strong six-fold sawtooth pattern in the torque, that is explained by rotation of the zigzag domains to minimize the magnetic interaction energy with the applied field. Modeling suggests that the sawtooth pattern arises in $R\bar{3}$ regions that are spatially separated from the C2 regions that generate the two-fold torque.
3. In the high-field intermediate field phase, there is a sinusoidal six-fold contribution to the torque that is opposite in sign to the predictions for a field-induced Kitaev state, but that may be due to fluctuating zigzag order, a finding which may have implications for the interpretation of zeros in the gap at the b -axes found by specific heat measurements [19].
4. A rather weak negative-slope feature at the C_2 -preserving b -axis (B1) does not follow the temperature and field dependence predicted for a Kitaev spin liquid in a magnetic field.
5. We see a sharp negative-slope feature near the B2 axis that does follow the predictions for a C_2 axis of a Kitaev spin liquid in a magnetic field, but B2 is not a C_2 axis, and moreover it and other similar features at lower fields may be due to domain switching in C2 regions of the crystal.

ACKNOWLEDGMENTS

This research was supported by the Natural Sciences and Engineering Research Council of Canada (NSERC RGPIN-2019-06446). S. Kim and Y.J. Kim acknowledge the Natural Sciences and Engineering Research Council of Canada (RGPIN-2019-06449, RTI-2019-00809), Canada Foundation for Innovation, and Ontario Research Fund. J. Gordon and H.Y. Kee acknowledge support from the Natural Sciences and Engineering Research Council of Canada Discovery Grant No. 2022-04601. H.Y. Kee also acknowledges the Canadian Institute for Advanced Research, and the Canada Research Chairs Program.

Appendix A: Thermal Cycling Effects

Most of our measurements on sample L7K were conducted during a single cooldown from room temperature (this was actually the second time the sample was cooled, the sample having come loose during the first cooldown, requiring re-mounting), but some followup measurements were carried out after thermally cycling the sample to room temperature and back to low temperature, and it was found that thermally cycling sample L7K once enhanced the 180° periodic contribution to the signal. As shown in Fig. 12, at 7 K after thermal cycling the 180° contribution is approximately twice as large as at 8 K before cycling. Fig. 12b shows the amplitude of the 180° periodic contribution, extracted by Fourier analysis, as a function of temperature. It can be seen that the 180° periodic contribution is enhanced at all measured temperatures. In contrast, a sinusoidal 60° periodic contribution to the signal (pink lines in Fig. 12d,f) is unaffected by thermally cycling the sample.

Further thermal-cycle measurements were conducted on sample L7K to comprehensively observe the effects of a thermal cycling, also shown in Fig. 12.

Inspection of the feature at the B2 axes shows that it is enhanced and shifted with thermal cycling. This, along with the analysis of §IV:B seen in Fig. 9f, would suggest an origin in the C2 regions of the crystal.

We notice for these successive thermal cyclings that the effect on the sample seems to have saturated - further cycling does not appear to noticeably further enhance the 180° periodic contribution, and continues to not effect the 60° periodic component in the paramagnetic and intermediate field regions. Within the zigzag phase at 4 T, however, the sawtooth signal loses much of its sharpness, and the 60° periodic contribution to the signal is diminished (Fig. 12a,b).

A possible explanation for these observations outside of the ordered phase, given the unaffected 60° component, is that there exist multiple phase separated regions of the sample. The C2 regions could be growing at the expense of the $R\bar{3}$ regions.

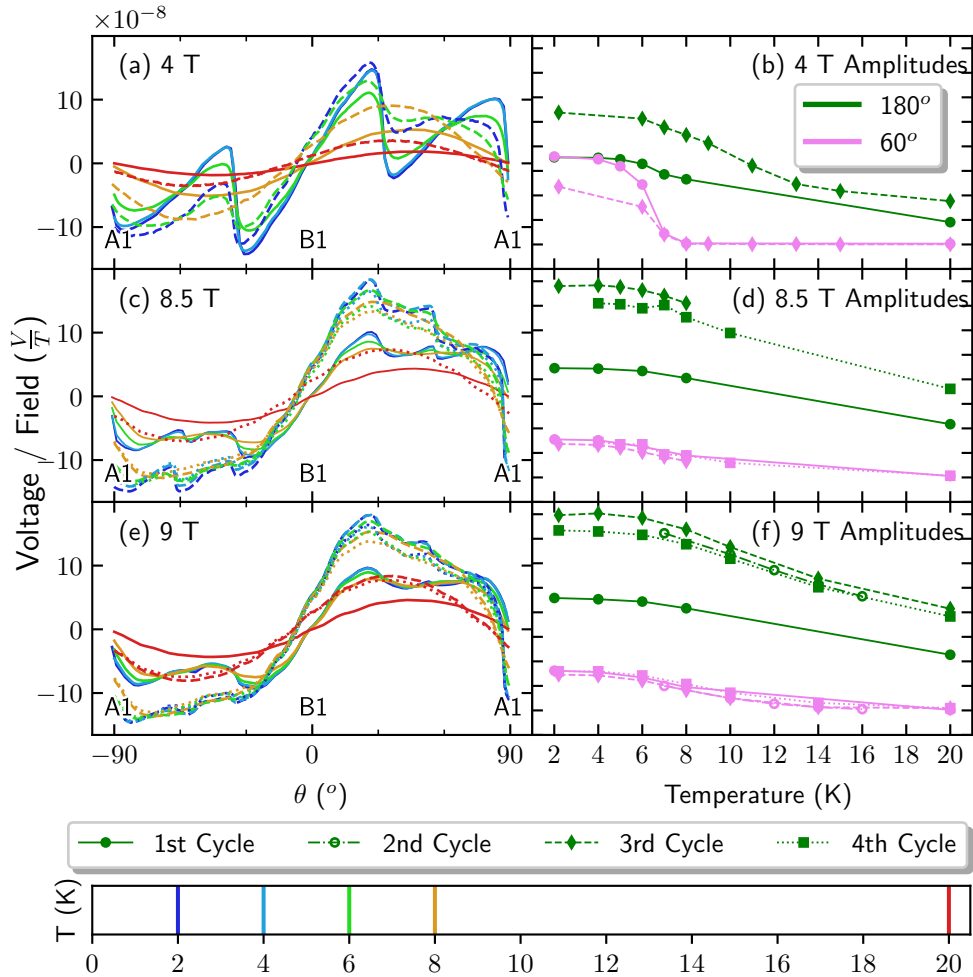


FIG. 12: (a), (c) and (e) show the raw angle-resolved torque at 4, 8.5 and 9 T respectively, after successive thermal cycles of the sample to room temperature and back down to ≈ 20 K, measured at 2, 4, 6, 8 and 20 K. (b), (d) and (f) show the corresponding Fourier amplitudes of the two-fold (180°) and six-fold (60°) components of the angle-resolved torque signal vs. temperature. The two-fold component of the signal is enhanced after thermally cycling the sample for all field strengths, though successive thermal cycles do not greatly affect the signal further. The six-fold component of the signal is not affected by thermally cycling the sample for field strengths outside of the antiferromagnetic ordered phase, though is clearly reduced within it (pink lines in (b)).

Regardless of the explanation, the lesson for subsequent measurements is to measure samples with the lowest possible levels of C2 contamination, to minimize thermal cycling, and perhaps to cool very slowly through the structural transition.

Within a given set of measurements (staying at low temperature) there was no sample history dependence that we observed from applying a field, rotating the sample in a field, or changing the temperature.

Appendix B: Comparisons of Sample Quality

Over time, the understanding of sample quality has evolved [28–30, 42] to capture the effects of stacking faults, and sample shape and size. A major distinction is

between samples in which zigzag order sets in at 7 K vs. ~ 14 K, which is now understood to reflect different stacking of the honeycomb planes [42]. The 7 K stacking has become the accepted ideal for experimental measurements [48], such crystals having what is believed to be the intrinsic stacking (ABCABC), whereas $T_N = 14$ K samples have an (ABAB) stacking.

A further distinction has recently been drawn [30], for 7 K samples, between those with $T_N < 7$ K and those with $7.2 \text{ K} < T_N < 7.5 \text{ K}$, the latter having a sharp structural transition at 140 K upon cooling, and in x-ray diffraction nearly pure $R\bar{3}$ symmetry at low temperature, while the former have a sluggish, broad structural transition below 140 K and in x-ray diffraction a mixture of $R\bar{3}$ and C2 regions at low temperature. The difference is probably in the density of stacking faults, as opposed to incorrectly

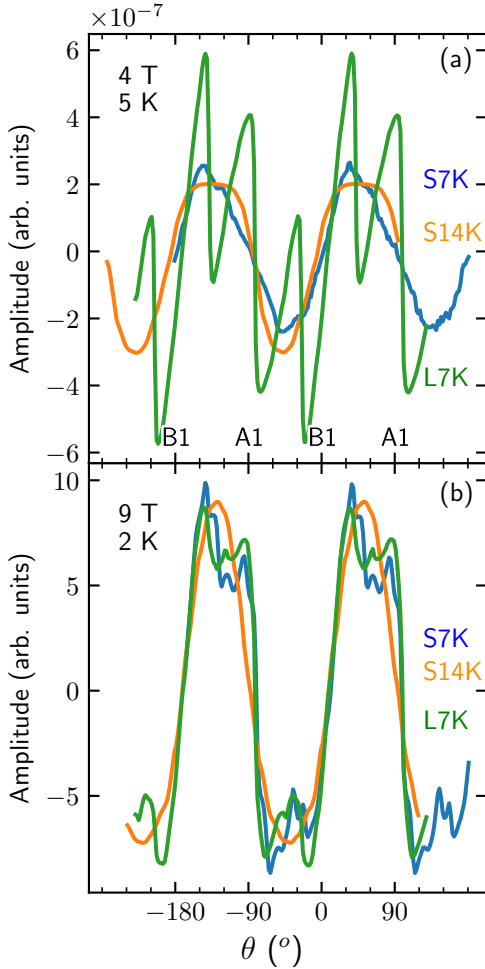


FIG. 13: Illustrating the differences between samples. (a) Torque vs. angle of samples S7K, S14K and L7K, at 4 T and 5 K. A multiplicative factor has been applied so that the amplitude of the 180° periodic contribution is the same across datasets. Only sample L7K shows a 60° periodic sawtooth, superposed on the 180° signal. (b) Angle-resolved torque response of samples S7K, S14K and L7K at 9 T and 2 K. Sample S14K shows only a 180° periodic contribution, while both samples S7K and L7K exhibit a complex series of higher-frequency contributions superposed on a strong 180° signal.

(ABAB) stacked regions.

As discussed in Appendix A, the 180° periodic signal is thus not intrinsic to the low-temperature structure of α - RuCl_3 , but rather indicates residual stacking faults, incorrect stacking, or strain within the sample. We note, moreover, that small crystals seem more disordered than our large crystal, regardless of T_N . Both a small $T_N = 7$ K sample (S7K) and a small $T_N = 14$ K sample (S14K) exhibit strong 180° periodic behaviour (see Fig. 13), but within the zigzag-ordered phase neither sample shows the clearly defined 60° periodic sawtooth signal of our large crystal L7K. A possible interpreta-

tion is that finite volume effects in small crystals inhibit domain rotation, although it is not clear if this is due to strong C_2 symmetry breaking, or a high density of defects that pin domain walls, or both. Similarly, Fig. 13(b) shows that the pure 180° periodic signal of sample S14K persists even into the ‘intermediate field phase’, where both S7K and sample L7K have developed additional features, including the prominent sinusoidal 60° signal discussed in the main body of this paper. From this we propose that the sinusoidal 60° periodic contribution to the angle-resolved torque, and by extension the presence of fluctuating zigzag order persisting beyond the boundary to the antiferromagnetically ordered phase, is an indicator of a sample with $T_N \sim 7$ K, although it may be that such a six-fold sinusoidal signal will appear in a 14 K sample at higher fields. We note in addition that of the 13 small samples we tested, 12 had predominantly $T_N \sim 14$ K transitions (some crystals had transitions at both 14 and 7 K), and only one had a pure 7 K transition.

Appendix C: Calibration

The cantilevers were measured in a low-temperature Wheatstone bridge configuration, via a 4-wire measurement. The measurements presented in this paper are given in volts, as measured across the Wheatstone bridge. A series of calibration measurements, with a known mass of 4.6 ± 0.1 mg of solder in zero-field conditions and at 2 and 20 K, was conducted to derive a conversion between volts and Nm. The mass was placed 590 ± 10 μm off-center on the cantilever to produce a twisting torque due to gravity. As a function of angle the calculated maximum torque for this calibration mass was $\tau = \vec{r} \times \vec{F}_g = (2.66 \pm 0.06) \times 10^{-8}$ Nm. The angle resolved torque of this calibration mass was measured and the result was fit with a sin function to determine the amplitude. The conversion was measured to be 2.77 ± 0.09 Nm/V, which together with the dimensions of the sample gives a torque-density conversion factor of $(17 \pm 4) \times 10^9$ Nm $^{-2}$ /V. At 4 T the maximum amplitude in our α - RuCl_3 measurements is approximately 1.5×10^{-7} V/T, which gives a magnetic moment of $(4.2 \pm 0.1) \times 10^{-7}$ Nm/T = $(4.5 \pm 0.1) \times 10^{16}$ μ_B . Given an estimated 16.3×10^{17} Ru atoms, this results in an estimated 0.028 ± 0.001 μ_B per Ru atom for the static moment, perpendicular to \vec{B} and the rotation axis.

The spring constant for the cantilever used in measuring sample L7K is $k = 9.3 \times 10^{-7}$ Nm/ $^\circ$. Together with the conversion factor and approximate maximum voltage measured of 8.9×10^{-7} V we find the maximum angular deflection of the cantilever in measurements to be $2.6 \pm 0.1^\circ$.

This maximum deflection allows us to estimate the torque interaction correction, $(\gamma/k)(\partial M/\partial \theta)B$ for our cantilever, where γ is the deflection angle. The condition for the torque interaction to be weak is for this factor to be small compared to 1 [36]. Even at the downward step of the sawtooth, where $\partial M/\partial \theta$ is largest, we find the fac-

tor to be quite small (~ 0.1 , or 10%). Everywhere else, in particular for purely sinusoidal signals, the correction is negligible. This means that the sharp features we observe in the angle resolved torque are due to the sample, and not due to non-linear torque interaction effects in the cantilever.

Appendix D: Confirming T_N

The rapid growth of the six-fold torque signal below 7 K, shown in Fig. 3b, is strong evidence that the magnetic phase transition took place at 7 K in sample LK7 for our first cooldown. Here we show torque at fixed angles, as a function of temperature, through 12 K and 7 K for sample L7K after the second cooldown (Fig. 14, unprimed labels) and after four cooldowns (Fig. 14, primed labels). Although the phase transition signature is not as clear, containing as they do a superposition of the 6-fold and 2-fold temperature dependence, these plots have the advantage of showing the temperature variation quasi-continuously, rather than at discrete points.

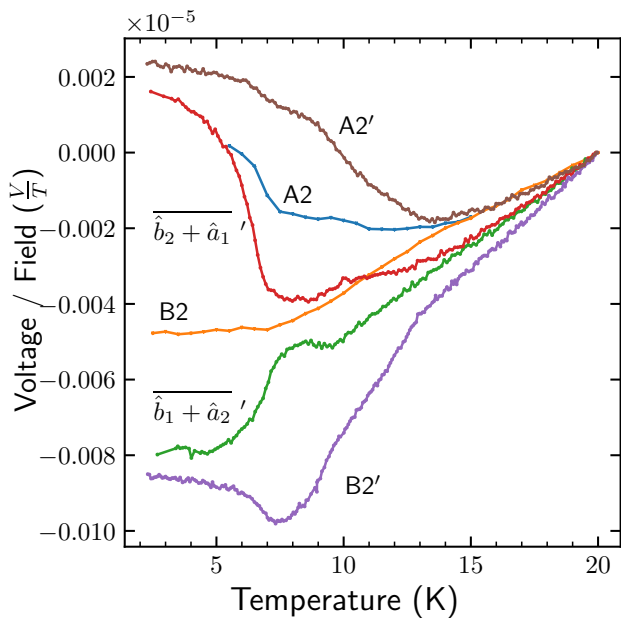


FIG. 14: Measurement of the angle resolved torque of sample L7K along and between high-symmetry directions, before and after (denoted by ') thermal cycling, at a constant field strength of 2 T (before) and 4 T (after). The measurements between symmetry axes were taken half-way between either the B2 and A1 axis (labeled $\overline{\hat{b}_2 + \hat{a}_1}'$), or B1 and A2 axes, (labeled $\overline{\hat{b}_1 + \hat{a}_2}'$). The result for each dataset at 20 K is used as a subtraction to better contrast the different responses. A clear kink-like feature is present at 7 K, consistent with the T_N seen in Fig. 3. After thermal cycling a feature is seen to develop at 13 K along some field directions.

For our first set of measurements, at 2 T the B2 curve shows a change of slope in the torque vs. temperature occurring at 7 K, although there is a suggestion of a change of slope at ~ 12 K as well. In the second, primed, set of measurements, taken at 4 T and after thermal cycling, the lower temperature feature is still intact, but a change of slope at ~ 12 K has become more prominent at some field-angles, with a possible further change at ~ 9 K.

Appendix E: Phase diagram of peaks

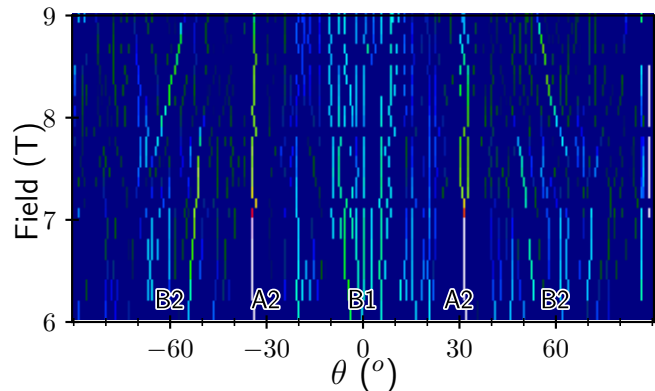


FIG. 15: A composite of the peaks in the (absolute value of) the derivative of the angle-resolved torque (ie. the magnetotropic coefficient) at 2 K at cross sections of field.

An analysis can be conducted of the peaks in the derivative of the angle-resolved torque by tracking their location in a magnetic field (T) vs. in-plane field angle (θ) phase diagram (see Fig. 15). These results can be compared to the phase boundaries of the zigzag 1 and zigzag 2 phases of Ref. [38], to which our Fig. 15 bears very little resemblance. This tells us that the additional steps that appear between about 6 T and 8 T are not due to crossing the boundary between zigzag phases 1 and 2; they are more likely due, as noted above, to domain switching in regions of the crystal where $R\bar{3}$ symmetry is broken.

Appendix F: Sample Alignment and Other Concerns

It was important to rule out the possibility that our observed two-fold anisotropy is due to misalignment of the sample, which is plausible given that there is approximately a factor of 10 difference in M/B between the in-plane and the c^* directions in α - RuCl_3 [44]. If the rotation axis is not precisely aligned with the c^* axis, then this large anisotropy will cause a two-fold torque to appear, even if the in-plane susceptibility is uniform.

We have tested this possibility numerically, using published M/B vs B data in the literature. Refs. [14, 38, 44]

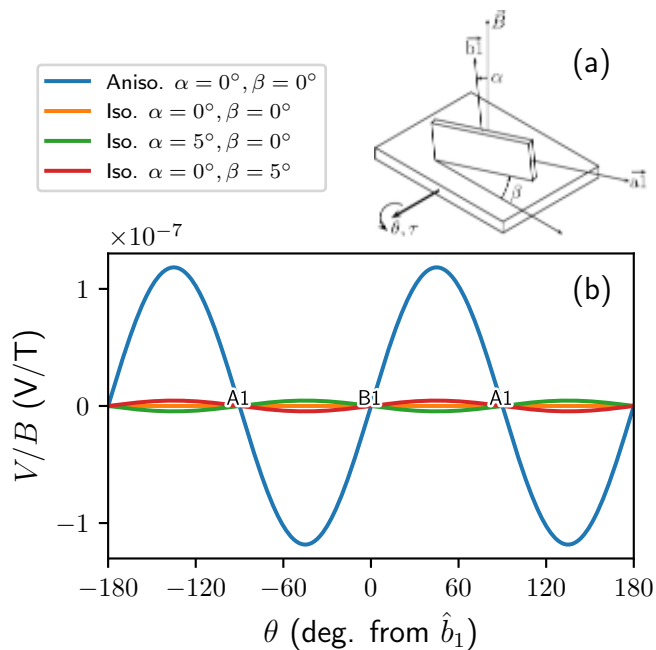


FIG. 16: (a) Cartoon schematic of misalignment angles α (rotation about the A1 axis), and β (rotation about the B1 axis). (b) Calculated in-plane torque, where the anisotropic result utilises the measured in-plane anisotropy of Kocsis [44] with no misalignment ($\alpha = \beta = 0$).

have published M/B as a function of field-angle, rotating the applied field both within the ab -plane, and from in-plane directions to the c^* -axis. All three papers find a two-fold in-plane anisotropy, but not only the magnitude but also the sign of the anisotropy differs between these papers: in [44] and [14] M/B is largest along B1, but in [38], Fig. 3g, M/B is largest at A1. This striking sample dependence reinforces the conclusion that the two-fold in-plane anisotropy of M/B is not intrinsic.

Our crystal L7K was oriented by eye, but the orienta-

tion was checked by comparing parallelism of the crystal facets with the sides of the rotation platform in a photograph of the mounted sample, and by using a microscope reticule and an x-y stage. The maximum misalignment has been assessed to be less than 2 degrees.

We characterize possible misalignment through two angles, α and β (see Fig. 16a). When $\alpha = \beta = 0$, the rotation axis is parallel to c^* , so that the B1 and A1 axes are perpendicular to the rotation axis. For Fig. 16b we have calculated the torque for four different cases, converting the calculated torque to voltage using the conversion factors in Appendix C, and scaling by $1/B$, for comparison to our measurements. Firstly, we used the two-fold anisotropy from [44] at 2 T and 5 T, interpolated to 4 T for comparison with our Fig. 3a, with no misalignment (i.e. $\alpha = \beta = 0$; blue curve in Fig. 16b). The magnitude of the V/B is very similar to what we observed in our first cool-down (see Fig. 3a). For the other, lower amplitude lines, we assumed that there is no in-plane two-fold anisotropy and calculated the torque: (i) with the sample perfectly aligned (that is, with B1 and A1 both perpendicular to the rotation/torque axis) which gives no two-fold torque (orange line); (ii) with $\alpha = 5^\circ, \beta = 0^\circ$ (green curve), and (iii) with $\alpha = 0^\circ, \beta = 5^\circ$ (red curve). The torque in these cases is more than a factor of ten too small to explain our observations, despite the misalignment angles being significantly larger than our estimated maximum misalignment. Note, too, that the α misalignment gives the wrong sign for the two-fold component of torque. We find that the β misalignment would have to be more than 10 degrees for the misalignment torque to become comparable in size to our measured two-fold torque, which is far beyond the upper limit on the actual misalignment. The misalignment torque is also too small to explain the change in the two-fold torque between our thermal cycling runs as arising from changing sample misalignment upon thermal cycling. Thus we conclude that the two-fold signal is due to in-plane magnetic anisotropy that is extrinsic in origin.

-
- [1] J. G. Rau, E. K.-H. Lee, and H.-Y. Kee, Spin-orbit physics giving rise to novel phases in correlated systems: Iridates and related materials, *Annu. Rev. Condens. Matter Phys.* **7**, 195 (2016).
- [2] I. Rousochatzakis, N. B. Perkins, Q. Luo, and H.-Y. Kee, Beyond kitaev physics in strong spin-orbit coupled magnets, *Rep. Prog. Phys.* **87**, 026502 (2024).
- [3] W. Witczak-Krempa, G. Chen, Y. B. Kim, and L. Balents, Correlated quantum phenomena in the strong spin-orbit regime, *Annu. Rev. Condens. Matter Phys.* **5**, 57 (2014).
- [4] T. Takayama, J. Chaloupka, A. Smerald, G. Khaliullin, and H. Takagi, Spin-orbit-entangled electronic phases in 4 d and 5 d transition-metal compounds, *J. Phys. Soc. Jpn.* **90**, 062001 (2021).
- [5] A. Kitaev, Anyons in an exactly solved model and beyond, *Ann. Phys.* **321**, 2 (2006).
- [6] M. Hermanns, I. Kimchi, and J. Knolle, Physics of the kitaev model: Fractionalization, dynamic correlations, and material connections, *Annu. Rev. Condens. Matter Phys.* **9**, 17 (2018).
- [7] H. Takagi, T. Takayama, G. Jackeli, G. Khaliullin, and S. E. Nagler, Concept and realization of kitaev quantum spin liquids, *Nat. Rev. Phys.* **1**, 264 (2019).
- [8] Y. Motome and J. Nasu, Hunting majorana fermions in kitaev magnets, *J. Phys. Soc. Jpn.* **89**, 012002 (2020).
- [9] S. M. Winter, Y. Li, H. O. Jeschke, and R. Valentí, Challenges in design of kitaev materials: Magnetic interactions from competing energy scales, *Phys. Rev. B* **93**, 214431 (2016).

- [10] S. M. Winter, A. A. Tsirlin, M. Daghofer, J. Van Den Brink, Y. Singh, P. Gegenwart, and R. Valentí, Models and materials for generalized kitaev magnetism, *J. Phys.: Condens. Matter* **29**, 493002 (2017).
- [11] J. G. Rau, E. K.-H. Lee, and H.-Y. Kee, Generic spin model for the honeycomb iridates beyond the kitaev limit, *Phys. Rev. Lett.* **112**, 077204 (2014), arXiv:1310.7940.
- [12] L. Janssen, E. C. Andrade, and M. Vojta, Magnetization processes of zigzag states on the honeycomb lattice: Identifying spin models for α -rucl3 and na2iro3, *Phys. Rev. B* **96**, 064430 (2017).
- [13] J. A. Sears, L. E. Chern, S. Kim, P. J. Bereciartua, S. Francoual, Y. B. Kim, and Y.-J. Kim, Ferromagnetic kitaev interaction and the origin of large magnetic anisotropy in α -rucl3, *Nat. Phys.* **16**, 837 (2020).
- [14] P. Lampen-Kelley, S. Rachel, J. Reuther, J.-Q. Yan, A. Banerjee, C. A. Bridges, H. B. Cao, S. E. Nagler, and D. Mandrus, Anisotropic susceptibilities in the honeycomb kitaev system α -rucl3, *Phys. Rev. B* **98**, 100403(R) (2018).
- [15] C. Balz, P. Lampen-Kelley, A. Banerjee, J. Yan, Z. Lu, X. Hu, S. M. Yadav, Y. Takano, Y. Liu, D. A. Tennant, M. D. Lumsden, D. Mandrus, and S. E. Nagler, Finite field regime for a quantum spin liquid in α -rucl3, *Phys. Rev. B* **100**, 060405(R) (2019).
- [16] J. A. Sears, Y. Zhao, Z. Xu, J. W. Lynn, and Y.-J. Kim, Phase diagram of α -rucl3 in an in-plane magnetic field, *Phys. Rev. B* **95**, 180411(R) (2017).
- [17] J. S. Gordon and H.-Y. Kee, Testing topological phase transitions in kitaev materials under in-plane magnetic fields: Application to α -rucl3, *Phys. Rev. Research* **3**, 013179 (2021).
- [18] K. Hwang, A. Go, J. H. Seong, T. Shibauchi, and E.-G. Moon, Identification of a kitaev quantum spin liquid by magnetic field angle dependence, *Nat. Commun.* **13**, 323 (2022).
- [19] O. Tanaka, Y. Mizukami, R. Harasawa, K. Hashimoto, K. Hwang, N. Kurita, H. Tanaka, S. Fujimoto, Y. Matsuda, E.-G. Moon, and T. Shibauchi, Thermodynamic evidence for a field-angle-dependent majorana gap in a kitaev spin liquid, *Nat. Phys.* **18**, 429 (2022).
- [20] Y. Kasahara, T. Ohnishi, Y. Mizukami, O. Tanaka, S. Ma, K. Sugii, N. Kurita, H. Tanaka, J. Nasu, Y. Motome, T. Shibauchi, and Y. Matsuda, Majorana quantization and half-integer thermal quantum hall effect in a kitaev spin liquid, *Nature* **559**, 227 (2018).
- [21] S.-H. Do, S.-Y. Park, J. Yoshitake, J. Nasu, Y. Motome, Y. S. Kwon, D. T. Adroja, D. J. Voneshen, K. Kim, T.-H. Jang, J.-H. Park, K.-Y. Choi, and S. Ji, Majorana fermions in the kitaev quantum spin system α -rucl3, *Nat. Phys.* **13**, 1079 (2017).
- [22] J. A. Sears, M. Songvilay, K. W. Plumb, J. P. Clancy, Y. Qiu, Y. Zhao, D. Parshall, and Y.-J. Kim, Magnetic order in α -rucl3: A honeycomb-lattice quantum magnet with strong spin-orbit coupling, *Phys. Rev. B* **91**, 144420 (2015).
- [23] S. Widmann, V. Tsurkan, D. A. Prishchenko, V. G. Mazurenko, A. A. Tsirlin, and A. Loidl, Thermodynamic evidence of fractionalized excitations in α -rucl3, *Phys. Rev. B* **99**, 094415 (2019).
- [24] J. A. N. Bruin, R. R. Claus, Y. Matsumoto, N. Kurita, H. Tanaka, and H. Takagi, Robustness of the thermal hall effect close to half-quantization in α -rucl3, *Nat. Phys.* **18**, 401 (2022).
- [25] Y. Kasahara, S. Suetsugu, T. Asaba, S. Kasahara, T. Shibauchi, N. Kurita, H. Tanaka, and Y. Matsuda, Quantized and unquantized thermal hall conductance of the kitaev spin liquid candidate α -rucl3, *Phys. Rev. B* **106**, L060410 (2022).
- [26] E. Lefrançois, G. Grissonnanche, J. Baglo, P. Lampen-Kelley, J.-Q. Yan, C. Balz, D. Mandrus, S. Nagler, S. Kim, Y.-J. Kim, N. Doiron-Leyraud, and L. Taillefer, Evidence of a phonon hall effect in the kitaev spin liquid candidate α -rucl3, *Phys. Rev. X* **12**, 021025 (2022).
- [27] P. Czajka, T. Gao, M. Hirschberger, P. Lampen-Kelley, A. Banerjee, N. Quirk, D. G. Mandrus, S. E. Nagler, and N. P. Ong, Planar thermal hall effect of topological bosons in the kitaev magnet α -rucl3, *Nat. Mater.* **22**, 36 (2023).
- [28] S. Kim, E. Horsley, C. Nelson, J. Ruff, and Y.-J. Kim, Re-investigation of moment direction in a kitaev material α -rucl3, arXiv:2403.04176 [cond-mat] (2024), arXiv:2403.04176 [cond-mat].
- [29] S. Kim, E. Horsley, J. P. C. Ruff, B. D. Moreno, and Y.-J. Kim, Structural transition and magnetic anisotropy in α -rucl3, *Phys. Rev. B* **109**, L140101 (2024).
- [30] H. Zhang, M. A. McGuire, A. F. May, H.-Y. Chao, Q. Zheng, M. Chi, B. C. Sales, D. G. Mandrus, S. E. Nagler, H. Miao, F. Ye, and J. Yan, Stacking disorder and thermal transport properties of α -rucl3, *Phys. Rev. Materials* **8**, 014402 (2024).
- [31] A. Banerjee, C. A. Bridges, J.-Q. Yan, A. A. Aczel, L. Li, M. B. Stone, G. E. Granroth, M. D. Lumsden, Y. Yiu, J. Knolle, S. Bhattacharjee, D. L. Kovrizhin, R. Moessner, D. A. Tennant, D. G. Mandrus, and S. E. Nagler, Proximate kitaev quantum spin liquid behaviour in a honeycomb magnet, *Nat. Mater.* **15**, 733 (2016).
- [32] K. A. Modic, M. D. Bachmann, B. J. Ramshaw, F. Arnold, K. R. Shirer, A. Estry, J. B. Betts, N. J. Ghimire, E. D. Bauer, M. Schmidt, M. Baenitz, E. Svanidze, R. D. McDonald, A. Shekhter, and P. J. W. Moll, Resonant torsion magnetometry in anisotropic quantum materials, *Nat. Commun.* **9**, 3975 (2018).
- [33] K. A. Modic, R. D. McDonald, J. P. C. Ruff, M. D. Bachmann, Y. Lai, J. C. Palmstrom, D. Graf, M. K. Chan, F. F. Balakirev, J. B. Betts, G. S. Boebinger, M. Schmidt, M. J. Lawler, D. A. Sokolov, P. J. W. Moll, B. J. Ramshaw, and A. Shekhter, Scale-invariant magnetic anisotropy in rucl3 at high magnetic fields, *Nat. Phys.* **17**, 240 (2021).
- [34] K. Riedl, Y. Li, S. M. Winter, and R. Valentí, Sawtooth torque in anisotropic $j_{\text{eff}} = 1/2$ magnets: Application to α -rucl3, *Phys. Rev. Lett.* **122**, 197202 (2019).
- [35] I. A. Leahy, C. A. Pocs, P. E. Siegfried, D. Graf, S.-H. Do, K.-Y. Choi, B. Normand, and M. Lee, Anomalous thermal conductivity and magnetic torque response in the honeycomb magnet α -rucl3, *Phys. Rev. Lett.* **118**, 187203 (2017).
- [36] J. Vanderkooy and W. R. Datars, Effects of sample rotation on de haas-van alphen oscillations, *Can. J. Phys.* **46**, 1215 (1968).
- [37] B. W. Lebert, S. Kim, D. A. Prishchenko, A. A. Tsirlin, A. H. Said, A. Alatas, and Y.-J. Kim, Acoustic phonon dispersion of α -rucl3, *Phys. Rev. B* **106**, L041102 (2022).
- [38] C. Balz, L. Janssen, P. Lampen-Kelley, A. Banerjee, Y. H. Liu, J.-Q. Yan, D. G. Mandrus, M. Vojta, and S. E. Nagler, Field-induced intermediate ordered phase

- and anisotropic interlayer interactions in α - rucl3, Phys. Rev. B **103**, 174417 (2021).
- [39] A. Banerjee, P. Lampen-Kelley, J. Knolle, C. Balz, A. A. Aczel, B. Winn, Y. Liu, D. Pajerowski, J. Yan, C. A. Bridges, A. T. Savici, B. C. Chakoumakos, M. D. Lumsden, D. A. Tennant, R. Moessner, D. G. Mandrus, and S. E. Nagler, Excitations in the field-induced quantum spin liquid state of α -rucl3, npj Quantum Mater. **3**, 8 (2018).
- [40] R. D. Johnson, S. C. Williams, A. A. Haghighirad, J. Singleton, V. Zapf, P. Manuel, I. I. Mazin, Y. Li, H. O. Jeschke, R. Valentí, and R. Coldea, Monoclinic crystal structure of α - rucl3 and the zigzag antiferromagnetic ground state, Phys. Rev. B **92**, 235119 (2015).
- [41] S.-Y. Park, S.-H. Do, K.-Y. Choi, D. Jang, T.-H. Jang, J. Scheffer, C.-M. Wu, J. S. Gardner, J. M. S. Park, J.-H. Park, and S. Ji, Emergence of the isotropic kitaev honeycomb lattice α -rucl₃ and its magnetic properties, J. Phys.: Condens. Matter **36**, 215803 (2024).
- [42] H. B. Cao, A. Banerjee, J.-Q. Yan, C. A. Bridges, M. D. Lumsden, D. G. Mandrus, D. A. Tennant, B. C. Chakoumakos, and S. E. Nagler, Low-temperature crystal and magnetic structure of α - rucl₃, Phys. Rev. B **93**, 134423 (2016).
- [43] C. Ritter, Zigzag type magnetic structure of the spin $j_{eff} = 1/2$ compound α -rucl₃ as determined by neutron powder diffraction, J. Phys.: Conf. Ser. **746**, 012060 (2016).
- [44] V. Kocsis, D. A. S. Kaib, K. Riedl, S. Gass, P. Lampen-Kelley, D. G. Mandrus, S. E. Nagler, N. Pérez, K. Nielsch, B. Büchner, A. U. B. Wolter, and R. Valentí, Magnetoelastic coupling anisotropy in the kitaev material α -rucl₃, Phys. Rev. B **105**, 094410 (2022).
- [45] J. Wagner, A. Sahasrabudhe, R. B. Versteeg, L. Wysocki, Z. Wang, V. Tsurkan, A. Loidl, D. I. Khomskii, H. Hedayat, and P. H. M. van Loosdrecht, Magneto-optical study of metamagnetic transitions in the antiferromagnetic phase of α -rucl₃, npj Quantum Mater. **7**, 1 (2022).
- [46] A. Banerjee, J. Yan, J. Knolle, C. A. Bridges, M. B. Stone, M. D. Lumsden, D. G. Mandrus, D. A. Tennant, R. Moessner, and S. E. Nagler, Neutron scattering in the proximate quantum spin liquid α -rucl₃, Science **356**, 1055 (2017).
- [47] A. N. Ponomaryov, E. Schulze, J. Wosnitza, P. Lampen-Kelley, A. Banerjee, J.-Q. Yan, C. A. Bridges, D. G. Mandrus, S. E. Nagler, A. K. Kolezhuk, and S. A. Zvyagin, Unconventional spin dynamics in the honeycomb-lattice material α -rucl₃: High-field electron spin resonance studies, Phys. Rev. B **96**, 241107(R) (2017).
- [48] S. Kim, B. Yuan, and Y.-J. Kim, α -rucl₃ and other kitaev materials, APL Mater. **10**, 080903 (2022).